

The discovery and characterization of minimoon 2024 PT₅

BRYCE T. BOLIN,^{1,*} LARRY DENNEAU,^{2,*} LAURA-MAY ABRON,³ ROBERT JEDICKE,²
KRISTIN CHIBOUCAS,⁴ CARL INGEBRETSEN,⁵ AND BRIAN C. LEMAUX^{4,6}

¹*Eureka Scientific, Oakland, CA 94602, U.S.A.*

²*Institute for Astronomy, University of Hawai'i at Mānoa, Honolulu, HI, 96822*

³*Griffith Observatory, Los Angeles, CA 90027*

⁴*Gemini Observatory/NSF NOIRLab, Hilo, HI, 96720, USA*

⁵*William H. Miller III Department of Physics and Astronomy, Johns Hopkins University, Baltimore, MD 21218, USA*

⁶*Department of Physics and Astronomy, University of California, Davis, One Shields Ave., Davis, CA 95616, USA*

(Received –; Revised –; Accepted –)

Submitted to ApJL

ABSTRACT

Minimoons are asteroids that become temporarily captured by the Earth-Moon system. We present the discovery of 2024 PT₅, a minimoon discovered by the Asteroid Terrestrial-impact Last Alert System (ATLAS) Sutherland telescope on 2024 August 7. The minimoon with heliocentric semi-major axis, $a \sim 1.01$ au, and perihelion, $q \sim 0.99$ au, became captured by the Earth-Moon system on 2024 September 29 and left on 2024 November 25 UTC. Visible g, r, i, and Z spectrophotometry was obtained using Gemini North/Gemini Multi-Object Spectrograph (GMOS) on 2024 September 27. The color indices are $g-r = 0.58 \pm 0.04$, $r-i = 0.29 \pm 0.04$, $i-Z = -0.27 \pm 0.06$, and the spectrum best matches lunar rock samples followed by S-complex asteroids. Assuming an albedo of 0.21 and using our measured absolute magnitude of 28.64 ± 0.04 , 2024 PT₅ has a diameter of 5.4 ± 1.2 m. We also detect variations in the lightcurve of 2024 PT₅ with a 0.28 ± 0.07 magnitude amplitude and a double-peaked period of $\sim 2600 \pm 500$ s. We improve the orbital solution of 2024 PT₅ with our astrometry and estimate the effect of radiation pressure on its deriving an area-to-mass ratio of $7.02 \pm 2.05 \times 10^{-5}$ m²/kg, implying a density of $\sim 3.9 \pm 2.1$ g/cm³, compatible with having a rocky composition. If we assume 2024 PT₅ is from the NEO population, its most likely sources are resonances in the inner Main Belt by comparing its orbit with the NEO population model, though this does not exclude a lunar origin.

Keywords: minor planets, asteroids: individual (2024 PT₅), temporarily captured orbiters, minimoons

1. INTRODUCTION

* These authors contributed equally to this manuscript.

Evidence from observations of near-Earth objects (NEOs) suggests that the majority originate from the Main Belt asteroids (MBAs) and Jupiter Family Comet (JFC) populations (Granvik et al. 2018; Nesvorný et al. 2023, 2024). A small percentage of NEOs can become temporary Earth co-orbitals, located in a 1:1 mean motion resonance with the Earth (Morais & Morbidelli 2002) where they can become Trojans or quasi-satellites of the Earth for several thousand years (Brasser et al. 2004). A small portion of NEOs, less than $< 10^{-7}$ of the total NEO population, can become temporarily captured by the Earth-Moon system’s gravity and enter its Hill sphere, becoming a so-called “minimoon” (Granvik et al. 2013; Jedicke et al. 2018).

Minimoons are captured at low relative velocities with the Earth-Moon system, less than 1 km/s, where they can be captured on timescales as long as 10s of days to years (Granvik et al. 2012; Fedorets et al. 2017). The first known minimoon, 2006 RH₁₂₀, remained in orbit around the Earth for ~ 400 days (Kwiatkowski et al. 2008), and the second, 2003 CD₃ was captured for ~ 900 days (Naidu et al. 2021) before escaping the Earth’s Hill sphere. Thus, the capture duration of minimoons represents a small portion of the time they share the Earth’s orbit.

While it is assumed that Earth co-orbitals such as minimoons are captured from the NEO population, emerging evidence suggests that some may originate as lunar impact ejecta. Ejecta from lunar impacts can be re-captured onto Earth-similar orbits where they can last for thousands of years (Gladman et al. 1995). Additionally, the observed spectral properties of some minimoons and quasi-satellites such as 2020 CD₃ and (469219) Kamo’oalewa resemble some lunar samples (Bolin et al. 2020; Sharkey et al. 2021). This evidence has led some to suggest a recent lunar impact as the origin for some Earth co-orbitals (e.g., Jiao et al. 2024)

This paper discusses the discovery of minimoon, 2024 PT₅, by the Asteroid Terrestrial-impact Last Alert System (ATLAS) telescope and observations taken at Gemini North. We will use the approach of Bolin et al. (2021, 2022, 2023) to use spectrophotometric observations at different visible wavelengths to constrain its physical properties as a test of whether 2024 PT₅ has an asteroidal or Lunar debris origin. We will also use the astrometry reported from our observations and the observations of others to refine the orbit of 2024 PT₅, measuring the effect of non-gravitational perturbations on its orbit (e.g., Micheli et al. 2012) and compare its orbit with the NEO population model (Morbidelli et al. 2020; Nesvorný et al. 2023).

2. OBSERVATIONS

The discovery observations of 2024 PT₅ were taken on 2024 August 7 21:11:57 UTC at the ATLAS Sutherland telescope, Minor Planet Center (MPC) observing code M22, (Fig. 1, Denneau et al. 2024). At the time of the asteroid’s discovery, the asteroid was located at right ascension (RA) = 18 57 04.97, dec = -55 56 00.24 and 1.54 lunar distances (0.00397 au) au from the Earth, a heliocentric distance of 1.017 au, at a phase angle of 128.747°, and had a visible magnitude of ~ 17 . The asteroid was detected in four 30 s ATLAS o-band filter exposures spaced over ~ 1700 s. The ATLAS o-band filter provides coverage between 560 nm and 820 nm with an effective wavelength of 663 nm (Tonry et al. 2018). The asteroid was moving 13.7°/d (0.57"/s) in the northwest direction at the time of discovery, resulting in having a trailed appearance in the ATLAS images (panels a, b, c, and d of Fig 1). The trailed exposures of 2024 PT₅ show little to no curvature over the 1700 s span of the discovery detections with a great circle residual of $\sim 1.2''$.

On 2024 September 27 05:54 UTC, 2024 PT₅ was observed using the 8.1 m Gemini North telescope with the Gemini Multi-Object Spectrograph (GMOS) instrument (Hook et al. 2004) in imaging mode

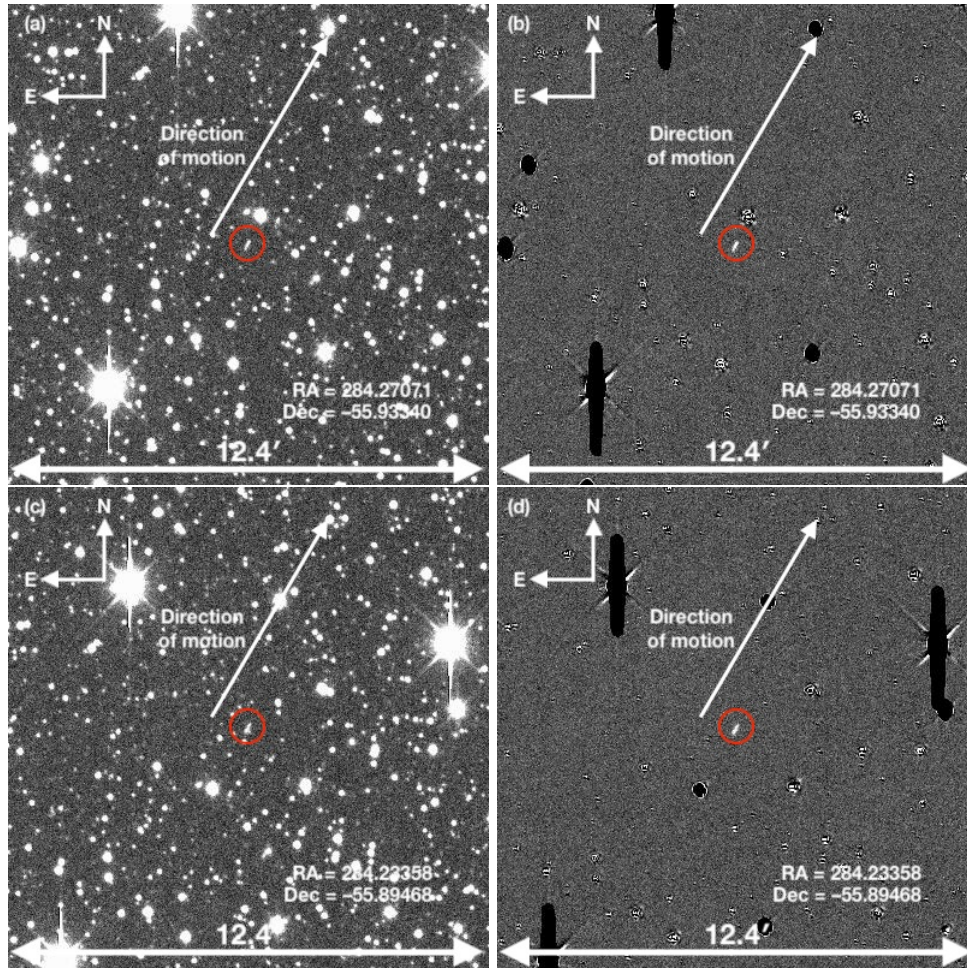


Figure 1. **Panel a:** The first of four o-band ATLAS-Sutherland telescope discovery images of 2024 PT₅ from 2024 August 7 21:11:57 UTC. The asteroid moved at a rate of 34.3 arcminutes per hour (13.7 degrees per day) in the northwest direction. The asteroid makes a ~ 9 pixel trail in the 30 s ATLAS exposures, indicated by the red circle. **Panel b:** the same as panel a but shows the image after subtracting static sources. Despite the presence of nearby stars, the asteroid is detected cleanly in the subtracted images. **Panel c:** the same as panel a, but the second of four o-band images containing 2024 PT₅ taken on 2024 August 7 21:16:35 UTC. **Panel d:** the same as panel c but shows the image after subtracting static sources. The asteroid was detected with an apparent magnitude of $m=17.13$ in panel b and $m=16.99$ in panel c. The large black areas in the subtracted images are regions of saturated pixels from bright stars. The direction of the asteroid and cardinal directions are indicated in each figure.

(Program ID GN-2024B-FT-106, PI B. Bolin). GMOS was used with the Hamamatsu array with an effective pixel scale of $0.0807''/\text{pixel}$ in 2×2 binning mode. The images were taken in Sloan Digital Sky Survey (SDSS)-equivalent g, r, and i filters (effective wavelengths 475 nm, 630 nm, and 780 nm, Fukugita et al. 1996). For coverage of the spectrum of 2024 PT₅ past 800 nm, we use the GMOS-N Z-band filter, which is effectively equivalent to the United Kingdom Infrared Telescope Wide-Field Camera (WFCAM) Z filter (Hewett et al. 2006). The WFCAM Z filter (effective wavelength 880 nm, Casali et al. 2007) was designed to be equivalent to the SDSS z filter (effective wavelength 890 nm) but avoids the atmospheric absorption band near 950 nm (Hodgkin et al. 2009).

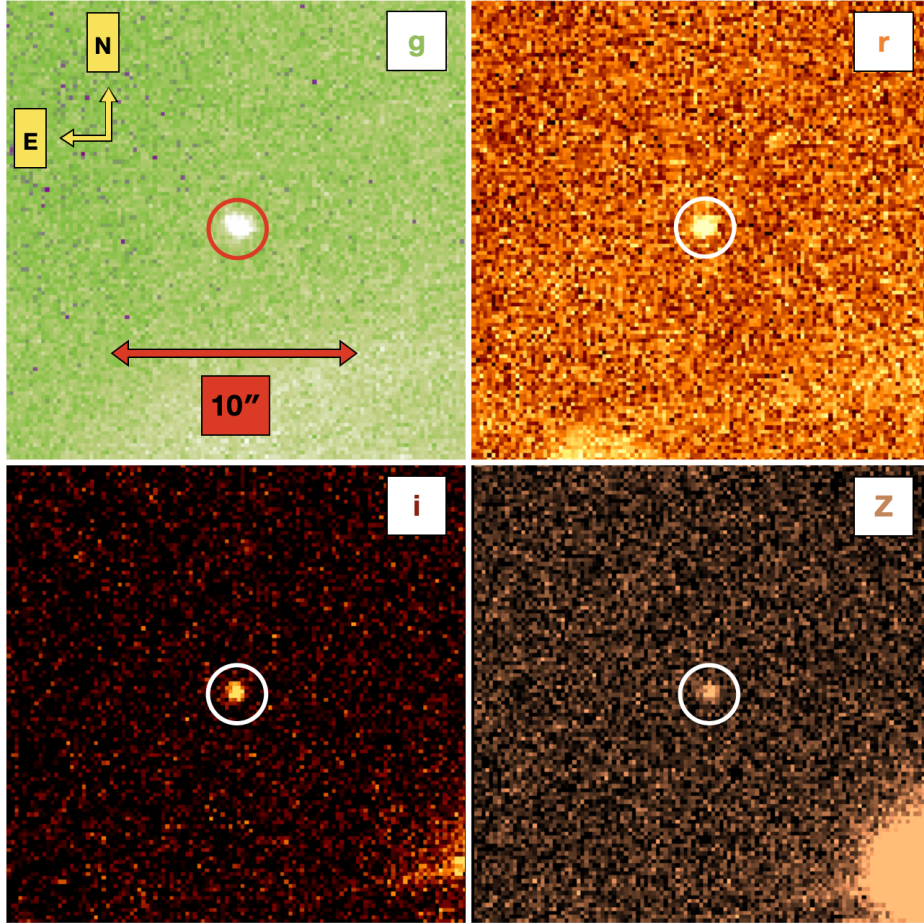


Figure 2. **Top left panel:** a median combination stack of 11 x 75 s g filter images of 2024 PT₅. An arrow indicating the width of 10'' is shown for scale, and the cardinal directions are indicated. **Top right panel:** a median combination stack of 5 x 50 s r filter images of 2024 PT₅. **Bottom left panel:** a median combination stack of 2 x 60 s i filter images of 2024 PT₅. **Bottom right panel:** a median combination stack of 2 x 60 s Z filter images of 2024 PT₅. The image scale and cardinal in the r, i, and Z stacks are the same as in the g image stack.

The observations of 2024 PT₅ with GMOS occurred when it was near RA = 16 59 59.22, dec = +67 01 25.5, 8.74 lunar distances from the Earth (0.0225 au), a heliocentric distance of 1.000 au, and had a phase angle of 84.4°. The seeing was $\sim 0.5\text{-}0.6''$ during the 2024 PT₅ observations as measured in g band images, and airmass ranged from 1.73 -1.91 during the ~ 40 minute observing sequence. During the sequence, we acquired 12 x 75 s g band exposures, 5 x 50 s r band exposures, 3 x 60 s i band exposures, and 3 x 90 s Z band exposures. Observations in the g, r, i, and Z filters were interspersed throughout the observation sequence to mitigate the effects of brightness variations in 2024 PT₅'s lightcurve on the color measurements. The telescope was tracked at the $\sim 93''/\text{h}$ rate of 2024 PT₅ during the exposures. Bias and flat frames were taken and used to detrend the images using the DRAGONS image pipeline (Labrie et al. 2023). Images of 2024 PT₅ when it intersected a background star were discarded. A mosaic of the separate g, r, i, and Z median-combined composite stacks of the 2024 PT₅ images are shown in Fig 2.

3. RESULTS

3.1. Astrometry and orbital determination

The astrometry from the Gemini North observations of 2024 PT₅ was measured with the Astrometrica software (Raab 2012) combined with reference stars from the *Gaia* data release 2 catalog (Gaia Collaboration et al. 2016, 2018). We conservatively estimate an astrometric uncertainty of 1.0'' in both the right ascension and declination directions in line with the typical astrometric precision for most ground-based measurements (e.g., Farnocchia et al. 2022). Additionally, the timing of the GMOS instrument is accurate to within a few tenths of a millisecond, inducing negligible effect on the astrometry¹.

The astrometry measured from the GMOS images was submitted to the MPC (Williams 2024). The GMOS astrometry of 2024 PT₅ was combined with 200 additional 2024 PT₅ observations taken independently by follow-up observers between 2024 August 7 UTC and 2024 October 24 UTC from the MPC archive². A complete table of the astrometry of 2024 PT₅ is provided in Table A1 of the appendix. We adopt conservative estimates for the astrometric uncertainties of $\sim 1.0''$ in both right ascension and declination for the other observatories' measured positions except for observations made at the Great Shefford Observatory in West Berkshire, England (MPC observatory code J95), where we used an estimated uncertainty of 0.4'' (Vereš et al. 2017).

Using the Find_Orb orbital determination software by Bill Gray³, we fit an orbit to the observations in Table A1, using the 8 planets and the Moon as perturbers, and including the effects of solar radiation pressure (e.g., Fedorets et al. 2020; Jewitt 2024). Our orbital fit results in estimates of the heliocentric and geocentric semi-major axis, a , eccentricity, e , inclination, i , ascending node, Ω , argument of perihelion, ω , mean anomaly, M , and the area-to-mass ratio (AMR) as a measure of the effect of solar radiation pressure on the orbit of 2024 PT₅.

The heliocentric, geocentric orbital parameters and area-to-mass ratio (a , e , i , Ω , ω , M , AMR) parameter estimates of the least square orbital fit using the observations of 2024 PT₅ is shown in Table 2. The mean observed-minus-computed residual from the least square fit using the 7-parameter fit is 0.33''. A complete list of the observed-minus-computed residuals in the along-track, $X_{res.}$, and cross-track, $Y_{res.}$, are shown in Table A1. The geocentric eccentricity e_g of 2024 PT₅ was ~ 1.05 on 2024 September 27 UTC, the date of the Gemini N observations, indicating that 2024 PT₅ was on a hyperbolic trajectory with respect to Earth. Its AMR of $7.02 \pm 2.05 \times 10^{-5}$ m²/kg is comparable to other small asteroids with measured AMRs (e.g., Micheli et al. 2013; Jedicke et al. 2018).

The orbital trajectory of 2024 PT₅ between 2024 June and 2025 April is shown in Fig. 3 based on values from JPL Horizons⁴. The e_g of 2024 PT₅ decreased below 1.0 at around 2024 September 29 23:40 UTC, as indicated by the red portion of the trajectory of 2024 PT₅ in the top and bottom panels of Fig. 3. The capture of 2024 PT₅ by the Earth-Moon system ended at around 2024 November 25 18:20, making it the most short-lived minimoon known, having been captured by the Earth-moon system for only ~ 60 days. Additionally, 2024 PT₅ did not make a complete revolution around the Earth-Moon barycenter, unlike previous minimoons such as 2006 RH₁₂₀ (Kwiatkowski et al. 2008; Granvik et al. 2012) and 2020 CD₃.

3.2. Photometry and spectral classification

¹ <https://www.gemini.edu/observing/phase-iii-retrieving-reducing-data/reducing-data/timing-information>

² https://minorplanetcenter.net/db_search/show_object?utf8=%E2%9C%93&object_id=2024+PT5, accessed on 2024 November 7.

³ https://www.projectpluto.com/find_orb.htm

⁴ <https://ssd.jpl.nasa.gov/horizons/app.html#/>

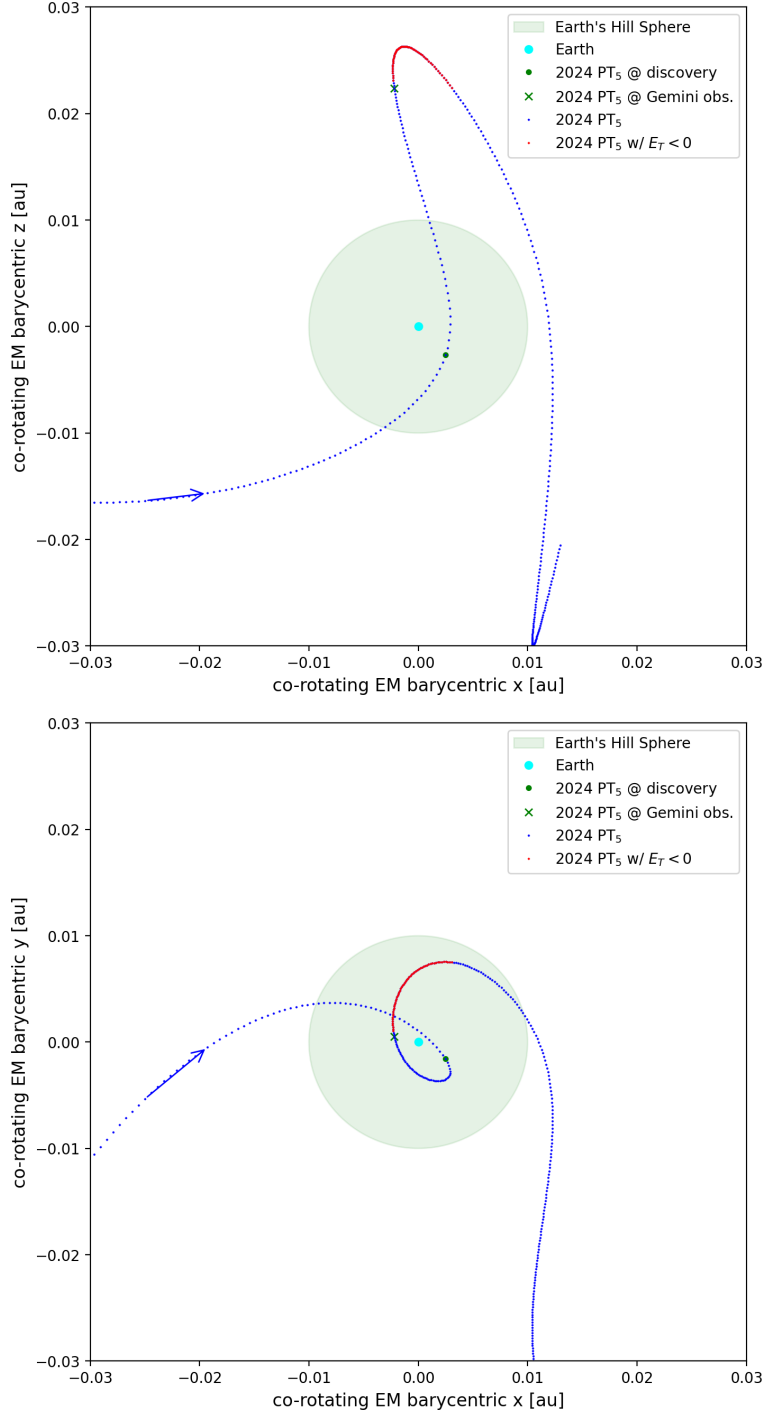


Figure 3. Top panel: side view of the Earth co-rotating frame orbital trajectory of 2024 PT₅ as it enters and leaves the Earth-Moon system between 2024 June and 2025 April in Cartesian Earth-Moon barycentric x and z coordinates. The daily position of 2024 PT₅ is represented as blue points except the portion of its trajectory when it had $e_g < 1$ plotted in red. The position of the Earth is plotted with a cyan circle. The circular green-shaded region indicates the Hill sphere of Earth. The position of 2024 PT₅, when it was discovered, is marked by a green circle, and the position of 2024 PT₅ when Gemini observed it is marked with a green X. A blue arrow indicates the direction of motion of 2024 PT₅ along its orbital path. **Bottom panel:** the same as the top panel, except in Cartesian Earth-Moon barycentric x and y coordinates.

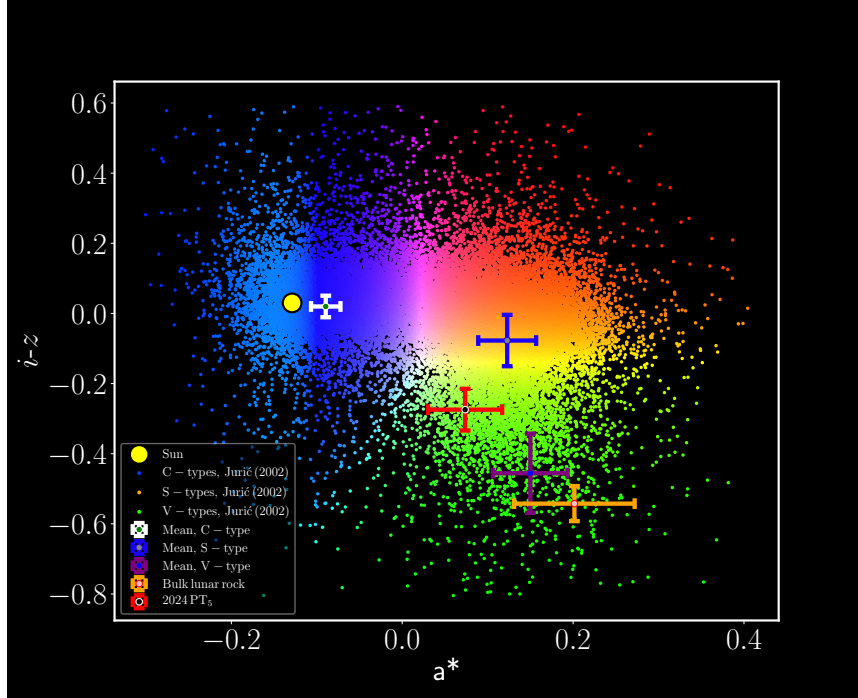


Figure 4. a^* vs. $i-z(Z)$ colors of 2024 PT₅ plotted with a^* vs. $i-z$ colors of C, S and V type asteroids from (Ivezić et al. 2001; Jurić et al. 2002), active comets (Solontoi et al. 2012), Kuiper Belt Objects (Ofek 2012), and bulk lunar rock samples (Isaacson et al. 2011). The colorization scheme of data points as a function of a^* and $i-z$ is adapted from Ivezić et al. (2002) where blue symbol colors correspond to C-type asteroids, red symbol colors correspond to S-type asteroids and green symbol colors correspond to V-type asteroids. We note that in this case the measured Z magnitude of 2024 PT₅ is plotted as a substitute for its z magnitude. $i-z$. The a^* and $i-z$ range of average S, V, and C-type asteroids are shown computed from the average spectra from DeMeo et al. (2009).

The photometry of 2024 PT₅ was measured using a 0.81'' aperture and then subtracting from it the median contribution from the sky background within a 1.3-2.4'' annulus. The g, r, i, and Z photometry were calibrated using solar analog stars from the Pan-STARRS catalog Chambers et al. (2016). The Pan-STARRS catalog magnitudes of the solar analog stars were transformed to SDSS magnitudes using the conversions from Tonry et al. (2012). We obtained brightnesses of $g = 23.52 \pm 0.03$, $r = 22.95 \pm 0.03$, $i = 22.66 \pm 0.03$, $Z = 22.93 \pm 0.05$. The multi-band colors of 2024 PT₅ are $g-r = 0.58 \pm 0.05$, $r-i = 0.29 \pm 0.04$, and $i-z = -0.27 \pm 0.06$. The $g-i$ color and spectra slope are 0.87 ± 0.04 and $9.5 \pm 1.1\%/100 \text{ nm}$.

Using the definition of a^* from Ivezić et al. (2001), $a^* = (0.89 (g-r)) + (0.45 (r-i)) - 0.57$, as an indicator of spectral slope, we find $a^* = 0.07 \pm 0.04$ as plotted vs. $i-z(Z)$ in Fig. 4. Overall, 2024 PT₅ has a^* and $i-z$ similar to S-types which have $a^* = 0.12 \pm 0.03$ and $i-z = -0.08 \pm 0.07$ on average and some V-type asteroids which have $a^* = 0.15 \pm 0.11$ and $i-z = -0.46 \pm 0.04$ on average as plotted in Fig. 4. 2024 PT₅ is redder compared with a smaller $i-z$ color compared to C-type asteroids, which have on average an $a^* = -0.09 \pm 0.02$ and $i-z = 0.02 \pm 0.03$ and the Sun, which has an $a^* = -0.13$ and $i-z = 0.03$.

We compute the spectral reflectance of 2024 PT₅ by dividing its flux per g, r, i, and Z filter obtained by the flux of a solar analog in a corresponding filter, normalizing it to a wavelength of 550 nm. The

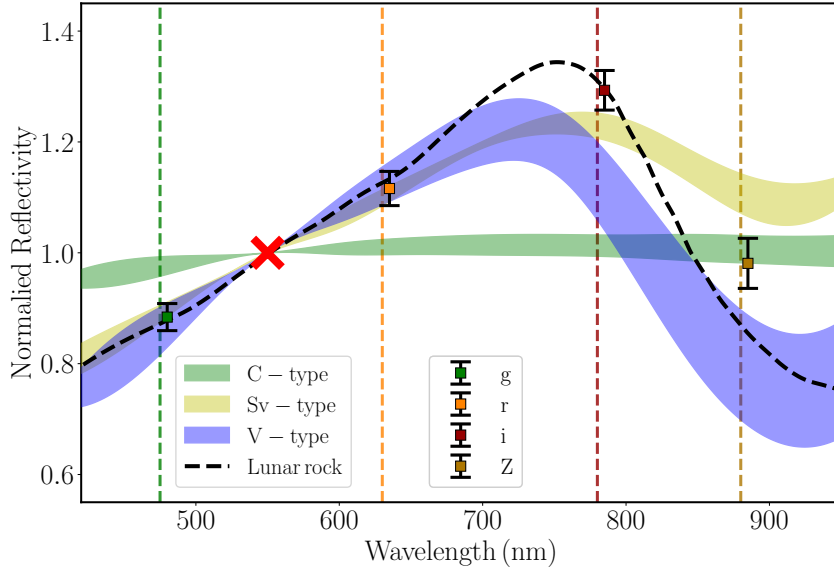


Figure 5. Reflectance photometric spectrum of 2024 PT₅ consisting of g, r, i, and Z observations of 2024 PT₅ on 2024 September 27 UTC. The λ_{eff} locations of the g, r, i, and Z filters have been plotted as vertical dashed lines. The data points for the normalized reflectivity of 2024 PT₅ have been offset slightly from their location in the wavelength direction. The error bars on the spectrum data points correspond to 1σ uncertainty. The spectrum has been normalized to unity at 550 nm, as indicated by the red cross. The spectral range of S, V and C-type asteroids from the Bus-DeMeo asteroid taxonomic catalog (DeMeo et al. 2009) are over-plotted with the V-type spectrum most closely resembling the spectra of 2024 PT₅. The average spectrum of Apollo program coarse bulk lunar rock samples is plotted for reference (Isaacson et al. 2011).

normalized reflectivity spectrum of 2024 PT₅ shown in Fig. 5 is similar to the spectra of S- and V-type asteroids (Bus & Binzel 2002; DeMeo et al. 2009) with a red slope between 470 nm and 770 nm and a decrease in reflectance near 880 nm. The spectrum of 2024 PT₅ is also similar to some bulk basaltic lunar rock samples consisting of pyroxene minerals (Isaacson et al. 2011). For a thorough comparison, we compute the χ^2 statistic for the spectrum of 2024 PT₅ compared to the spectrum of 19 different asteroid types including S-complex asteroid types (S, Sq, Sv, Q), C-complex types (B, C, Cg, Cgh), X-complex types (X, Xc, Xe, Xk, Xn), and other assorted types (A, D, K, L, O, R, V) from (Bus & Binzel 2002; DeMeo et al. 2009). We find the closest match is to lunar rock with a reduced χ^2 of 2.76 and Sv-type asteroids with a reduced χ^2 of 3.75. By comparison, the comparison with V-type spectra results in a reduced χ^2 of ~ 12.84 .

We use our g and r magnitude measurements of 2024 PT₅ to estimate an equivalent V-band brightness of 23.2 ± 0.04 on 2024 September 7. We calculated the H magnitude of 2024 PT₅ using our estimated V magnitude and the phase function from equation from Bowell et al. (1988):

$$H = V - 5 \log_{10}(r_h \Delta) + 2.5 \log_{10} [(1 - G) \Phi_1(\alpha) + G \Phi_2(\alpha)] \quad (1)$$

where r_h is the 1.000 au heliocentric distance, Δ is its geocentric distance of 0.0225 au and α is its phase angle of 84.4° of 2024 PT₅ on 2024 September 27 UTC. G is the phase coefficient which we use the value of 0.2, the average value for S-type asteroids (Vereš et al. 2015). $\Phi_1(\alpha)$ and $\Phi_2(\alpha)$ are the

basis functions normalized at $\alpha = 0^\circ$ described in (Bowell et al. 1988). We obtain $H = 28.64 \pm 0.04$ but caution that the uncertainty on H is underestimated due to the lack of information about the phase function.

3.3. Lightcurve, periodicity, and axial ratio

We use the g filter data to search for periodic variations in the time series brightness of 2024 PT₅. The measured time series photometric values in the individual g images are presented in Table 2 and plotted in the top panel of Fig. 6. There are variations as large as ~ 0.2 - 0.25 magnitudes in the brightness of 2024 PT₅, significantly larger than the ~ 0.01 magnitude variations seen in Skyprobe data for 2024 September 27 UTC⁵ and the ~ 0.05 mag uncertainty of the individual g filter data points.

The Lomb-Scargle periodogram (Lomb 1976) was applied to the time series g filter data, as seen in the top panel of Fig. 7. We take a similar approach as Bolin et al. (2024) to estimating the uncertainty on the determined period by removing \sqrt{N} data points from the time series lightcurve and repeating our periodogram estimation of the lightcurve period 10,000 times, resulting in a central value of ~ 1317 s and a 1σ uncertainty estimate of ~ 227 s. We apply phase dispersion minimization analysis to our data (Stellingwerf 1978) as an independent check of the Lomb-Scargle results, obtaining a result of ~ 1150 s as seen in the bottom panel of Fig. 7, comparable with the lightcurve period estimate. These period estimates imply that 2024 PT₅ has a double-peaked rotation period of $\sim 2600 \pm 500$ s.

Using the observed amplitude of the g filter lightcurve of $0.28 \sim 0.07$, we estimate the rough shape of 2024 PT₅ assuming it is a prolate triaxial ellipsoid with dimensions $a:b:c$, where $b \geq a \simeq c$ in rough agreement with the shapes of other asteroids inferred from lightcurve inversion (e.g., Hanuš et al. 2016; Hanuš et al. 2018). The ratio between b/a is described by $b/a = 10^{0.4A}$ where A is the peak-to-trough lightcurve amplitude (Binzel et al. 1989) and assuming $a \simeq c$, resulting in a $b/a \sim 1.3$. However, the axial ratio may be exaggerated due to the effect of observing at a large phase angle of $\sim 84^\circ$ on 2024 September 27 UTC (Zappala et al. 1990) as has been suggested for lightcurve observations of other small solar system objects (e.g., Bolin et al. 2018).

4. DISCUSSION AND CONCLUSIONS

The spectrum of 2024 PT₅ is similar to asteroids from the S-complex, as well as some samples of lunar rock, which suggests that it may either originate from the inner Main Belt, where the majority of S-type asteroids are found (DeMeo & Carry 2014), or as a piece of debris resulting from an impact on the moon ejected into an Earth-similar orbit (Gladman et al. 1995). We can use the orbital information of 2024 PT₅ as an additional constraint on its likely origin and physical properties through comparison with dynamical models describing the escape of asteroids from the Main Belt into the NEO population (Granvik et al. 2017; Nesvorný et al. 2023).

We use the visible albedos, p_v , measured for S-complex and lunar rock samples to estimate the albedo of 2024 PT₅. S-complex asteroids have an albedo of ~ 0.21 (Thomas et al. 2011), while lunar rock has an albedo of ~ 0.14 (Matthews 2008). As an independent albedo estimate, we compare the orbit of 2024 PT₅ with the NEOMOD3 population model suggests its most likely source is the ν_6 resonance located near the inner edge of the Main Belt with an 88.4% probability. The next most likely location, with a 11% chance of 2024 PT₅ coming from it, is the 3:1 mean motion

⁵ <https://www.cfht.hawaii.edu/cgi-bin/elixir/skyprobe.pl?plot&mcal.20240927.png>

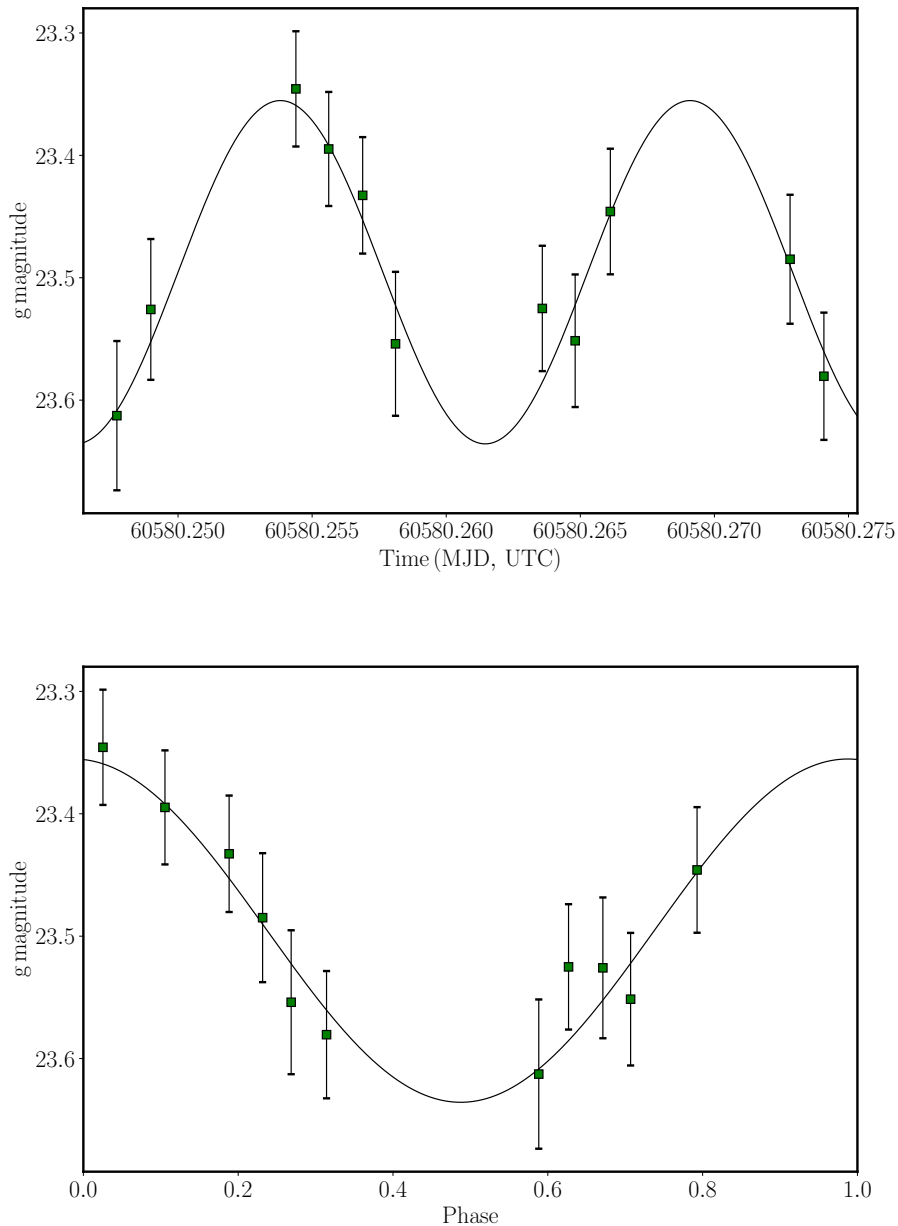


Figure 6. Top panel: g filter lightcurve from 2024 September 27 GMOS observations of 2024 PT₅. The error bars on the data points are equal to their 1σ photometric uncertainties. A model lightcurve is plotted in black with a double-peaked period of ~ 2600 s and amplitude of 0.28 magnitudes. **Bottom panel:** phased g filter lightcurve data of 2024 PT₅ using a lightcurve period of ~ 1300 s and amplitude of 0.28 magnitude.

resonance located in the Main Belt at 2.5 au. Weighing the NEO albedo model (Morbidelli et al. 2020) according to these source probabilities for 2024 PT₅ results in a predicted p_v of ~ 0.21 . We assuming a conservative albedo estimate of ~ 0.1 corresponding to the scatter in albedo measurements for small S-complex asteroids (Delbo et al. 2003; Binzel et al. 2004).

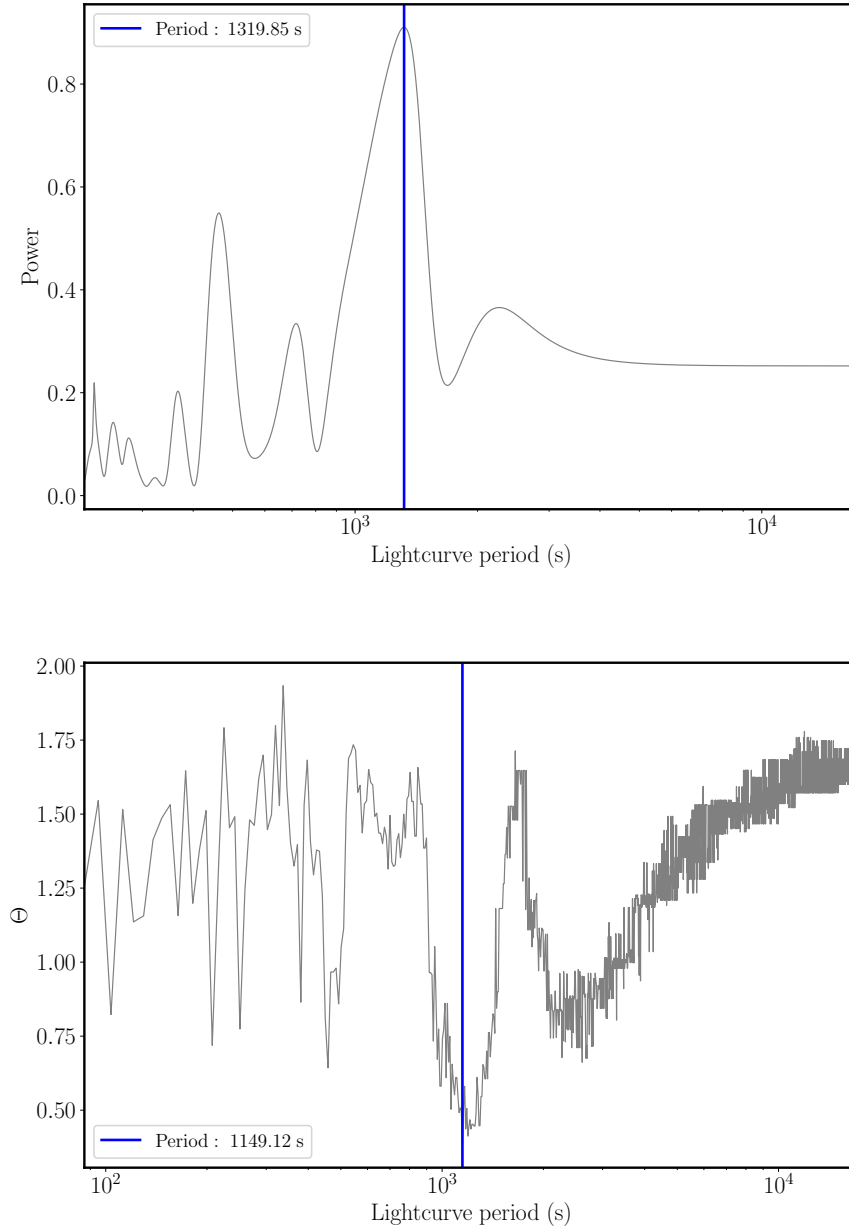


Figure 7. Top panel: Lomb-Scargle periodogram of lightcurve period vs. spectral power (Lomb 1976) for the g filter data from the 2024 September 27 UTC Gemini N/GMOS observations. A peak in the power is located at single-peaked lightcurve period of 1320 s. Bottom panel: Phase dispersion minimization analysis of lightcurve rotation period vs. Θ metric (Stellingwerf 1978). The Θ metric is minimized at single-peaked rotation periods of 1150 s similar to the 1320 ± 227 s period found with the Lomb-Scargle Periodogram.

We use the albedo estimate and H magnitude of 2024 PT₅ to determine the diameter, D, of 2024 PT₅ using the equation $D = \frac{1329}{\sqrt{p_v}} 10^{-\frac{H}{5}}$ from Russell (1916) arriving at $D = 5.4 \pm 1.2$ m. Combining this diameter calculation with the AMR determined from our orbital fit, we can estimate a bulk density for 2024 PT₅ of $3.9 \pm 2.1 \text{ g/cm}^3$ comparable with achondritic basaltic meteorites (Macke et al. 2011)

and small asteroids with AMR measurements (Mommert et al. 2014). If we use the mean albedo of lunar rock samples of 0.14, we obtain an diameter of 6.0 ± 1.7 m and a bulk density of 3.6 ± 2.4 g/cm³. This density estimate is comparable to the density of some lunar rock samples (Kiefer et al. 2012). Using these density estimates, the mass of 2024 PT₅ is $\sim 10^5$ kg. With the comparison of its physical properties determined from our observations to the physical properties of asteroids and lunar samples, we conclude that 2024 PT₅ the physical properties of 2024 PT₅ deduced from our observations is compatible within an inner Main Belt or lunar ejecta origin.

ACKNOWLEDGMENTS

This study is based on observations obtained at the international Gemini Observatory, a program of NSF’s NOIRLab, which is managed by the Association of Universities for Research in Astronomy (AURA) under a cooperative agreement with the National Science Foundation on behalf of the Gemini Observatory partnership.

Gemini Observatory is located on Maunakea, land of the Kānaka Maoli people, and a mountain of considerable cultural, natural, and ecological significance to the indigenous Hawaiian people. The authors wish to acknowledge the importance and reverence of Maunakea and express gratitude for the opportunity to conduct observations from the mountain.

Facility: Gemini North

REFERENCES

- Binzel, R. P., Farinella, P., Zappalà, V., & Cellino, A. 1989, in *Asteroids II*, ed. R. P. Binzel, T. Gehrels, & M. S. Matthews, 416–441
- Binzel, R. P., Rivkin, A. S., Stuart, J. S., et al. 2004, *Icarus*, 170, 259, doi: [10.1016/j.icarus.2004.04.004](https://doi.org/10.1016/j.icarus.2004.04.004)
- Bolin, B. T., Ghosal, M., & Jedicke, R. 2024, *MNRAS*, 527, 1633, doi: [10.1093/mnras/stad3227](https://doi.org/10.1093/mnras/stad3227)
- Bolin, B. T., Noll, K. S., Caiazzo, I., Fremling, C., & Binzel, R. P. 2023, *Icarus*, 400, 115562, doi: [10.1016/j.icarus.2023.115562](https://doi.org/10.1016/j.icarus.2023.115562)
- Bolin, B. T., Weaver, H. A., Fernandez, Y. R., et al. 2018, *ApJL*, 852, L2, doi: [10.3847/2041-8213/aaa0c9](https://doi.org/10.3847/2041-8213/aaa0c9)
- Bolin, B. T., Fremling, C., Holt, T. R., et al. 2020, *ApJL*, 900, L45, doi: [10.3847/2041-8213/abae69](https://doi.org/10.3847/2041-8213/abae69)
- Bolin, B. T., Fernandez, Y. R., Lisse, C. M., et al. 2021, *AJ*, 161, 116, doi: [10.3847/1538-3881/abd94b](https://doi.org/10.3847/1538-3881/abd94b)
- Bolin, B. T., Ahumada, T., van Dokkum, P., et al. 2022, *MNRAS*, 517, L49, doi: [10.1093/mnrasl/slac089](https://doi.org/10.1093/mnrasl/slac089)
- Bowell, E., Hapke, B., Domingue, D., et al. 1988, *Asteroids II*, 399
- Brasser, R., Innanen, K. A., Connors, M., et al. 2004, *Icarus*, 171, 102, doi: [10.1016/j.icarus.2004.04.019](https://doi.org/10.1016/j.icarus.2004.04.019)
- Bus, S. J., & Binzel, R. P. 2002, *Icarus*, 158, 146, doi: [10.1006/icar.2002.6856](https://doi.org/10.1006/icar.2002.6856)
- Casali, M., Adamson, A., Alves de Oliveira, C., et al. 2007, *A&A*, 467, 777, doi: [10.1051/0004-6361:20066514](https://doi.org/10.1051/0004-6361:20066514)
- Chambers, K. C., Magnier, E. A., Metcalfe, N., et al. 2016, *ArXiv e-prints*, <https://arxiv.org/abs/1612.05560>
- Delbo, M., Harris, A. W., Binzel, R. P., Pravec, P., & Davies, J. K. 2003, *Icarus*, 166, 116, doi: [10.1016/j.icarus.2003.07.002](https://doi.org/10.1016/j.icarus.2003.07.002)
- DeMeo, F. E., Binzel, R. P., Slivan, S. M., & Bus, S. J. 2009, *Icarus*, 202, 160, doi: [10.1016/j.icarus.2009.02.005](https://doi.org/10.1016/j.icarus.2009.02.005)
- DeMeo, F. E., & Carry, B. 2014, *Nature*, 505, 629, doi: [10.1038/nature12908](https://doi.org/10.1038/nature12908)
- Denneau, L., Siverd, R., Tonry, J., et al. 2024, *Minor Planet Electronic Circulars*, 2024-P170
- Farnocchia, D., Reddy, V., Bauer, J. M., et al. 2022, *Planetary Science Journal*, 3, 156, doi: [10.3847/PSJ/ac7224](https://doi.org/10.3847/PSJ/ac7224)

- Fedorets, G., Granvik, M., & Jedicke, R. 2017, *Icarus*, 285, 83, doi: [10.1016/j.icarus.2016.12.022](https://doi.org/10.1016/j.icarus.2016.12.022)
- Fedorets, G., Micheli, M., Jedicke, R., et al. 2020, *AJ*, 160, 277, doi: [10.3847/1538-3881/abc3bc](https://doi.org/10.3847/1538-3881/abc3bc)
- Fukugita, M., Ichikawa, T., Gunn, J. E., et al. 1996, *AJ*, 111, 1748, doi: [10.1086/117915](https://doi.org/10.1086/117915)
- Gaia Collaboration, Prusti, T., de Bruijne, J. H. J., et al. 2016, *A&A*, 595, A1, doi: [10.1051/0004-6361/201629272](https://doi.org/10.1051/0004-6361/201629272)
- Gaia Collaboration, Brown, A. G. A., Vallenari, A., et al. 2018, *A&A*, 616, A1, doi: [10.1051/0004-6361/201833051](https://doi.org/10.1051/0004-6361/201833051)
- Gladman, B. J., Burns, J. A., Duncan, M. J., & Levison, H. F. 1995, *Icarus*, 118, 302, doi: [10.1006/icar.1995.1193](https://doi.org/10.1006/icar.1995.1193)
- Granvik, M., Jedicke, R., Bolin, B., Chyba, M., & Patterson, G. 2013, *Earth's Temporarily-Captured Natural Satellites - The First Step towards Utilization of Asteroid Resources*, ed. V. Badescu, 151–167
- Granvik, M., Morbidelli, A., Vokrouhlický, D., et al. 2017, *A&A*, 598, A52, doi: [10.1051/0004-6361/201629252](https://doi.org/10.1051/0004-6361/201629252)
- Granvik, M., Vaubaillon, J., & Jedicke, R. 2012, *Icarus*, 218, 262, doi: [10.1016/j.icarus.2011.12.003](https://doi.org/10.1016/j.icarus.2011.12.003)
- Granvik, M., Morbidelli, A., Jedicke, R., et al. 2018, *Icarus*, 312, 181, doi: [10.1016/j.icarus.2018.04.018](https://doi.org/10.1016/j.icarus.2018.04.018)
- Hanuš, J., Delbo, M., Alí-Lagoa, V., et al. 2018, *Icarus*, 299, 84, doi: [10.1016/j.icarus.2017.07.007](https://doi.org/10.1016/j.icarus.2017.07.007)
- Hanuš, J., Delbo, M., Vokrouhlický, D., et al. 2016, *A&A*, 592, A34, doi: [10.1051/0004-6361/201628666](https://doi.org/10.1051/0004-6361/201628666)
- Hewett, P. C., Warren, S. J., Leggett, S. K., & Hodgkin, S. T. 2006, *MNRAS*, 367, 454, doi: [10.1111/j.1365-2966.2005.09969.x](https://doi.org/10.1111/j.1365-2966.2005.09969.x)
- Hodgkin, S. T., Irwin, M. J., Hewett, P. C., & Warren, S. J. 2009, *MNRAS*, 394, 675, doi: [10.1111/j.1365-2966.2008.14387.x](https://doi.org/10.1111/j.1365-2966.2008.14387.x)
- Hook, I. M., Jørgensen, I., Allington-Smith, J. R., et al. 2004, *PASP*, 116, 425, doi: [10.1086/383624](https://doi.org/10.1086/383624)
- Isaacson, P. J., Pieters, C. M., Besse, S., et al. 2011, *Journal of Geophysical Research (Planets)*, 116, E00G11, doi: [10.1029/2010JE003731](https://doi.org/10.1029/2010JE003731)
- Ivezić, Ž., Tabachnik, S., Rafikov, R., et al. 2001, *AJ*, 122, 2749, doi: [10.1086/323452](https://doi.org/10.1086/323452)
- Ivezić, Ž., Lupton, R. H., Jurić, M., et al. 2002, *AJ*, 124, 2943, doi: [10.1086/344077](https://doi.org/10.1086/344077)
- Jedicke, R., Bolin, B. T., Bottke, W. F., et al. 2018, *Frontiers in Astronomy and Space Sciences*, 5, 13, doi: [10.3389/fspas.2018.00013](https://doi.org/10.3389/fspas.2018.00013)
- Jewitt, D. 2024, arXiv e-prints, arXiv:2411.10923, doi: [10.48550/arXiv.2411.10923](https://doi.org/10.48550/arXiv.2411.10923)
- Jiao, Y., Cheng, B., Huang, Y., et al. 2024, *Nature Astronomy*, 8, 819, doi: [10.1038/s41550-024-02258-z](https://doi.org/10.1038/s41550-024-02258-z)
- Jurić, M., Ivezić, Ž., Lupton, R. H., et al. 2002, *AJ*, 124, 1776, doi: [10.1086/341950](https://doi.org/10.1086/341950)
- Kiefer, W. S., Macke, R. J., Britt, D. T., Irving, A. J., & Consolmagno, G. J. 2012, *Geophys. Res. Lett.*, 39, L07201, doi: [10.1029/2012GL051319](https://doi.org/10.1029/2012GL051319)
- Kwiatkowski, T., Kryszczynska, A., Polinska, M., et al. 2008, *LPI Contributions*, 1405, 8297
- Labrie, K., Simpson, C., Cardenas, R., et al. 2023, *Research Notes of the American Astronomical Society*, 7, 214, doi: [10.3847/2515-5172/ad0044](https://doi.org/10.3847/2515-5172/ad0044)
- Lomb, N. R. 1976, *Ap&SS*, 39, 447, doi: [10.1007/BF00648343](https://doi.org/10.1007/BF00648343)
- Macke, R. J., Britt, D. T., & Consolmagno, G. J. 2011, *M&PS*, 46, 311, doi: [10.1111/j.1945-5100.2010.01155.x](https://doi.org/10.1111/j.1945-5100.2010.01155.x)
- Matthews, G. 2008, *ApOpt*, 47, 4981, doi: [10.1364/AO.47.004981](https://doi.org/10.1364/AO.47.004981)
- Micheli, M., Tholen, D. J., & Elliott, G. T. 2012, *NewA*, 17, 446, doi: [10.1016/j.newast.2011.11.008](https://doi.org/10.1016/j.newast.2011.11.008)
- . 2013, *Icarus*, 226, 251, doi: [10.1016/j.icarus.2013.05.032](https://doi.org/10.1016/j.icarus.2013.05.032)
- Mommert, M., Hora, J. L., Farnocchia, D., et al. 2014, *ApJ*, 786, 148, doi: [10.1088/0004-637X/786/2/148](https://doi.org/10.1088/0004-637X/786/2/148)
- Morais, M. H. M., & Morbidelli, A. 2002, *Icarus*, 160, 1, doi: [10.1006/icar.2002.6937](https://doi.org/10.1006/icar.2002.6937)
- Morbidelli, A., Delbo, M., Granvik, M., et al. 2020, *Icarus*, 340, 113631, doi: [10.1016/j.icarus.2020.113631](https://doi.org/10.1016/j.icarus.2020.113631)
- Naidu, S. P., Micheli, M., Farnocchia, D., et al. 2021, *ApJL*, 913, L6, doi: [10.3847/2041-8213/abf836](https://doi.org/10.3847/2041-8213/abf836)
- Nesvorný, D., Deienno, R., Bottke, W. F., et al. 2023, *AJ*, 166, 55, doi: [10.3847/1538-3881/ace040](https://doi.org/10.3847/1538-3881/ace040)
- Nesvorný, D., Vokrouhlický, D., Shelly, F., et al. 2024, *Icarus*, 417, 116110, doi: [10.1016/j.icarus.2024.116110](https://doi.org/10.1016/j.icarus.2024.116110)
- Ofek, E. O. 2012, *The Astrophysical Journal*, 749, 10

- Raab, H. 2012, *Astrometrica: Astrometric data reduction of CCD images*.
<http://ascl.net/1203.012>
- Russell, H. N. 1916, *ApJ*, 43, 173,
doi: [10.1086/142244](https://doi.org/10.1086/142244)
- Sharkey, B. N. L., Reddy, V., Malhotra, R., et al. 2021, *Communications Earth and Environment*, 2, 231, doi: [10.1038/s43247-021-00303-7](https://doi.org/10.1038/s43247-021-00303-7)
- Solontoi, M., Ivezić, Ž., Jurić, M., et al. 2012, *Icarus*, 218, 571,
doi: [10.1016/j.icarus.2011.10.008](https://doi.org/10.1016/j.icarus.2011.10.008)
- Stellingwerf, R. F. 1978, *ApJ*, 224, 953,
doi: [10.1086/156444](https://doi.org/10.1086/156444)
- Thomas, C. A., Trilling, D. E., Emery, J. P., et al. 2011, *AJ*, 142, 85,
doi: [10.1088/0004-6256/142/3/85](https://doi.org/10.1088/0004-6256/142/3/85)
- Tonry, J. L., Stubbs, C. W., Lykke, K. R., et al. 2012, *ApJ*, 750, 99,
doi: [10.1088/0004-637X/750/2/99](https://doi.org/10.1088/0004-637X/750/2/99)
- Tonry, J. L., Denneau, L., Heinze, A. N., et al. 2018, *PASP*, 130, 064505,
doi: [10.1088/1538-3873/aabadf](https://doi.org/10.1088/1538-3873/aabadf)
- Vereš, P., Jedicke, R., Fitzsimmons, A., et al. 2015, *Icarus*, 261, 34,
doi: [10.1016/j.icarus.2015.08.007](https://doi.org/10.1016/j.icarus.2015.08.007)
- Vereš, P., Farnocchia, D., Chesley, S. R., & Chamberlin, A. B. 2017, *Icarus*, 296, 139,
doi: [10.1016/j.icarus.2017.05.021](https://doi.org/10.1016/j.icarus.2017.05.021)
- Williams, G. V. 2024, *Minor Planet Electronic Circulars*, 2024-V67
- Zappala, V., Cellino, A., Barucci, A. M., Fulchignoni, M., & Lupishko, D. F. 1990, *A&A*, 231, 548

Table 1. Orbital elements of 2024 PT₅ based on observations collected between 2024 August 7 UTC and 2020 October 24 UTC. The orbital elements are shown for the Julian date (JD) using the software `Find_Orb` by Bill Gray. The 1σ uncertainties are given in parentheses.

Heliocentric Elements	
Epoch (JD)	2,460,607.5
Time of perihelion, T_p (JD)	$2,460,638.2598770 \pm (5.58 \times 10^{-5})$
Semi-major axis, a (au)	$1.0121184340 \pm (2.03 \times 10^{-8})$
Eccentricity, e	$0.021315140 \pm (3.89 \times 10^{-8})$
Perihelion, q (au)	$0.9905449810 \pm (3.01 \times 10^{-8})$
Aphelion, Q (au)	$1.0336918860 \pm (5.53 \times 10^{-8})$
Inclination, i ($^\circ$)	$1.5167380 \pm (4.7 \times 10^{-6})$
Ascending node, Ω ($^\circ$)	$304.494733 \pm (9.0 \times 10^{-5})$
Argument of perihelion, ω ($^\circ$)	$117.54969 \pm (1.0 \times 10^{-4})$
Mean Anomaly, M ($^\circ$)	$330.225693 \pm (5.4 \times 10^{-5})$
Geocentric Elements	
Epoch (JD)	2,460,607.5
Time of perihelion, $T_{p,g}$ (JD)	$2,460,429.570191 \pm (2.87 \times 10^{-4})$
Semi-major axis, a_g (au)	$0.017623959 \pm (1.09 \times 10^{-7})$
Eccentricity, e_g	$0.61405662 \pm (2.04 \times 10^{-6})$
Perihelion, q_g (au)	$0.006801850 \pm (7.1 \times 10^{-8})$
Aphelion, Q_g (au)	$0.028446068 \pm (1.56 \times 10^{-7})$
Inclination, i_g ($^\circ$)	$105.640940 \pm (4.0 \times 10^{-5})$
Ascending node, Ω_g ($^\circ$)	$302.876944 \pm (3.40 \times 10^{-4})$
Argument of perihelion, ω_g ($^\circ$)	$277.668305 \pm (3.9 \times 10^{-4})$
Mean Anomaly, M_g ($^\circ$)	$129.9004 \pm (1.0 \times 10^{-3})$
Area-to-Mass ratio, AMR (m^2/kg)	$7.02 \times 10^{-5} \pm (2.05 \times 10^{-5})$
Absolute Magnitude, H	$28.64 \pm (0.04)$

Table 2. Summary of 2024 PT₅ photometry taken on 2024 September 27 UTC.

Date ¹ (MJD UTC)	Filter ²	Exp ³ (s)	m^4
60580.2477197	g	75 s	23.61 ± 0.06
60580.2489847	g	75 s	23.53 ± 0.06
60580.2543947	g	75 s	23.35 ± 0.05
60580.2556186	g	75 s	23.39 ± 0.05
60580.2568848	g	75 s	23.43 ± 0.05
60580.2581092	g	75 s	23.55 ± 0.06
60580.2635833	g	75 s	23.53 ± 0.05
60580.2648080	g	75 s	23.55 ± 0.05
60580.2661196	g	75 s	23.45 ± 0.05
60580.2728218	g	75 s	23.48 ± 0.05
60580.2740833	g	75 s	23.58 ± 0.05

Table 2. Columns: (1) observation date correct for light travel time; (2) Gemini N/GMOS Filter; (3) Exposure time (4) per filter apparent magnitude with 1 σ uncertainties

APPENDIX

Table A1. Summary of astrometry from observations taken by Gemini North/GMOS and other observatories between 2024 August 7 UTC and 2024 October 24 UTC.

Date ¹ (UTC)	R.A. ²	Dec. ³	$\sigma_{\text{R.A.}}$ ⁴ ($''$)	$\sigma_{\text{Dec.}}$ ⁵ ($''$)	$X_{\text{res.}}$ ⁶ ($''$)	$Y_{\text{res.}}$ ⁷ ($''$)	Obs. code ⁸
2024 8 7.883302	18 57 04.97	-55 56 00.24	1	1	0.42	-0.3	M22
2024 8 7.886527	18 56 56.059	-55 53 40.85	1	1	0.3	-0.04	M22
2024 8 7.892126	18 56 40.711	-55 49 37.52	1	1	0.37	0.05	M22
2024 8 7.903165	18 56 10.685	-55 41 31.85	1	1	-0.64	-0.03	M22
2024 8 12.060358	18 14 04.848	-09 25 00.44	1	1	0.13	0.29	W68
2024 8 12.065029	18 13 59.82	-09 22 24.35	1	1	0.27	-0.4	W68
2024 8 12.070721	18 13 53.688	-09 19 13.58	1	1	0.28	-0.88	W68
2024 8 12.105146	18 13 17.028	-08 59 51.4	1	1	-0.23	0.13	W68
2024 8 12.319011	18 12 25.265	-07 31 12.58	1	1	0.01	-0.43	T08
2024 8 12.321781	18 12 22.212	-07 29 42.04	1	1	0.12	-0.56	T08
2024 8 12.329519	18 12 13.702	-07 25 27.95	1	1	0.11	0.04	T08
2024 8 12.341403	18 12 00.773	-07 18 58.54	1	1	0.03	-0.36	T08
2024 8 12.890515	18 09 43.9	-02 45 25.0	1	1	0.13	0.1	I93
2024 8 12.892993	18 09 41.83	-02 44 10.7	1	1	0.42	0.07	I93
2024 8 12.896212	18 09 39.07	-02 42 34.8	1	1	-0.38	-0.56	I93
2024 8 12.90611	18 08 55.59	-02 37 52.5	1	1	-0.19	0.48	M45
2024 8 12.90899	18 08 53.62	-02 36 25.8	1	1	-0.03	0.62	M45
2024 8 12.91187	18 08 51.68	-02 34 59.5	1	1	0.26	0.39	M45
2024 8 12.912952	18 09 30.362	-02 36 41.8	0.4	0.4	0.25	0.11	J95
2024 8 12.914243	18 09 29.386	-02 36 03.24	0.4	0.4	0.21	0.07	J95
2024 8 12.916158	18 09 27.936	-02 35 06.0	0.4	0.4	0.07	0.05	J95
2024 8 12.916981	18 09 27.326	-02 34 41.34	0.4	0.4	0.19	0.11	J95
2024 8 12.92071	18 08 49.26	-02 30 57.2	1	1	-0.11	0.52	L04
2024 8 12.92166	18 09 03.22	-02 29 37.2	1	1	-0.69	-0.06	126
2024 8 12.92453	18 08 46.74	-02 29 02.7	1	1	-0.28	0.5	L04
2024 8 12.925395	18 09 19.685	-02 30 30.96	1	1	0.01	0.24	Z80
2024 8 12.92612	18 08 45.73	-02 28 14.9	1	1	0.06	0.65	L04
2024 8 12.928026	18 09 00.72	-02 26 59.4	1	1	0.29	0.06	203
2024 8 12.92976	18 08 43.4	-02 26 26.1	1	1	0.18	0.42	L04
2024 8 12.930038	18 09 16.248	-02 28 13.04	1	1	-0.52	-0.48	Z80
2024 8 12.933006	18 08 57.61	-02 24 38.1	1	1	0.29	0.17	204
2024 8 12.934692	18 09 12.878	-02 25 53.69	1	1	-0.38	-0.04	Z80
2024 8 12.93511	18 08 53.09	-02 22 55.3	1	1	-0.16	0.4	126

Continued on next page

Table A1 – *Continued from previous page*

Date ¹ (UTC)	R.A. ²	Dec. ³	$\sigma_{\text{R.A.}}$ ⁴ (")	$\sigma_{\text{Dec.}}$ ⁵ (")	$X_{\text{res.}}$ ⁶ (")	$Y_{\text{res.}}$ ⁷ (")	Obs. code ⁸
2024 8 12.93542	18 08 55.23	-02 23 17.9	1	1	0.07	-0.11	203
2024 8 12.93627	18 08 55.21	-02 23 00.8	1	1	0.32	0.24	204
2024 8 12.939514	18 08 52.88	-02 21 23.5	1	1	0.22	-0.23	204
2024 8 12.942278	18 08 50.3	-02 19 53.6	1	1	0.29	0.08	203
2024 8 12.94275	18 08 50.56	-02 19 47.0	1	1	0.33	0.02	204
2024 8 12.945971	18 08 48.28	-02 18 10.9	1	1	0.05	-0.56	204
2024 8 13.01645	18 09 01.788	-01 10 9.24	1	1	-0.33	-0.11	Y05
2024 8 13.018163	18 09 00.034	-01 09 18.53	1	1	0.31	-0.24	Y05
2024 8 13.019828	18 08 58.4	-01 08 29.81	1	1	0.34	-0.07	Y05
2024 8 13.10167	18 08 34.805	+00 23 28.32	1	1	-0.28	0.71	W68
2024 8 13.104829	18 08 31.841	+00 21 56.3	1	1	0.11	-0.54	W68
2024 8 13.110256	18 08 26.88	+00 19 20.93	1	1	0.11	0.46	W68
2024 8 13.120185	18 08 17.878	+00 14 33.76	1	1	-0.14	0.88	W68
2024 8 13.179412	18 07 28.721	+00 13 41.99	1	1	-0.39	-0.15	W68
2024 8 13.179862	18 07 28.368	+00 13 53.76	1	1	0.01	-0.41	W68
2024 8 13.180313	18 07 28.058	+00 14 06.32	1	1	0.48	-0.2	W68
2024 8 130.4929	18 08 31.937	+00 09 03.1	1	1	0.73	-0.6	U52
2024 8 13.21124	18 08 30.293	+00 08 07.84	1	1	0.12	0.15	U52
2024 8 13.21319	18 08 28.594	+00 07 11.46	1	1	0.14	-0.95	U52
2024 8 13.239647	18 09 08.398	+00 15 40.75	1	1	-0.53	0.23	T08
2024 8 13.240107	18 09 07.91	+00 15 55.01	1	1	-0.49	-0.33	T08
2024 8 13.241031	18 09 07.02	+00 16 20.71	1	1	-0.06	-0.29	T08
2024 8 13.393218	18 06 40.975	+01 27 26.89	1	1	0.26	-0.47	T08
2024 8 13.393681	18 06 40.608	+01 27 39.46	1	1	0.11	0.24	T08
2024 8 13.394144	18 06 40.21	+01 27 52.92	1	1	0.02	-0.35	T08
2024 8 13.394605	18 06 39.818	+01 28 05.02	1	1	-0.07	-0.01	T08
2024 8 13.395066	18 06 39.427	+01 28 18.05	1	1	-0.22	-0.62	T08
2024 8 13.395503	18 06 40.692	+01 27 53.75	1	1	-0.61	0.37	T05
2024 8 13.395955	18 06 40.289	+01 28 07.18	1	1	0.38	-0.34	T05
2024 8 13.396407	18 06 39.979	+01 28 18.91	1	1	0.29	-0.99	T05
2024 8 13.396858	18 06 39.598	+01 28 30.68	1	1	0.36	-0.57	T05
2024 8 13.39731	18 06 39.228	+01 28 43.54	1	1	0.36	0.23	T05
2024 8 13.495137	18 07 16.651	+02 06 36.61	1	1	-0.16	0.02	Q06
2024 8 13.502696	18 07 10.0	+02 10 02.57	1	1	-0.28	0.16	Q06
2024 8 13.510252	18 07 03.417	+02 13 28.4	1	1	0.02	-0.01	Q06
2024 8 13.818888	18 06 10.31	+04 26 07.1	1	1	-0.18	-0.02	L01
2024 8 13.820447	18 06 09.1	+04 26 47.6	1	1	-0.11	-0.04	L01
2024 8 13.822003	18 06 07.91	+04 27 28.0	1	1	-0.26	0.42	L01

Continued on next page

Table A1 – *Continued from previous page*

Date ¹ (UTC)	R.A. ²	Dec. ³	$\sigma_{\text{R.A.}}$ ⁴ (")	$\sigma_{\text{Dec.}}$ ⁵ (")	$X_{\text{res.}}$ ⁶ (")	$Y_{\text{res.}}$ ⁷ (")	Obs. code ⁸
2024 8 13.8344	18 06 00.492	+04 30 42.59	1	1	-0.07	0.34	G19
2024 8 13.84207	18 05 55.073	+04 34 00.77	1	1	-0.29	-0.02	G19
2024 8 13.846848	18 05 53.06	+04 38 40.8	1	1	-0.14	0.25	104
2024 8 13.850708	18 05 50.09	+04 40 20.6	1	1	0.05	0.57	104
2024 8 13.85616	18 05 45.182	+04 40 04.01	1	1	0.03	-0.04	G19
2024 8 13.86987	18 05 35.688	+04 45 55.08	1	1	-0.54	0.32	G19
2024 8 13.89015	18 05 21.965	+04 54 32.83	1	1	-0.38	0.51	G19
2024 8 13.89554	18 05 18.427	+04 56 49.96	1	1	-0.28	0.09	G19
2024 8 13.99644	18 04 13.93	+05 41 28.8	1	1	-0.14	-0.13	K83
2024 8 13.9989	18 04 12.77	+05 42 28.8	1	1	-0.1	0.03	K83
2024 8 14.872873	18 02 20.237	+11 24 21.74	0.4	0.4	-0.21	-0.11	J95
2024 8 14.875193	18 02 18.746	+11 25 12.4	0.4	0.4	-0.14	-0.07	J95
2024 8 14.87675	18 01 52.49	+11 26 12.8	1	1	0.01	-0.1	G02
2024 8 14.876922	18 02 17.647	+11 25 50.27	0.4	0.4	0.1	-0.55	J95
2024 8 14.879154	18 02 16.234	+11 26 39.01	0.4	0.4	-0.15	-0.12	J95
2024 8 14.88029	18 01 50.38	+11 27 29.0	1	1	-0.02	0.1	G02
2024 8 14.937552	18 01 41.203	+11 51 18.89	1	1	-0.02	-0.15	Y89
2024 8 14.942425	18 01 37.93	+11 53 02.12	1	1	-0.19	0.45	Y89
2024 8 14.947234	18 01 34.727	+11 54 43.23	1	1	-0.06	0.57	Y89
2024 8 15.75102	18 00 18.23	+16 56 43.87	1	1	-0.24	0.32	M49
2024 8 15.75565	18 00 14.654	+16 58 16.18	1	1	-0.17	0.09	M49
2024 8 15.840247	17 59 17.45	+16 54 19.4	1	1	-0.26	-0.17	G34
2024 8 15.84308	17 59 19.699	+16 55 38.57	1	1	0.15	-0.3	K87
2024 8 15.847264	17 59 13.29	+16 56 29.4	1	1	-0.21	-0.36	G34
2024 8 15.849602	17 59 11.94	+16 57 12.6	1	1	-0.2	-0.32	G34
2024 8 15.851941	17 59 10.54	+16 57 55.8	1	1	0.24	0.03	G34
2024 8 15.85295	17 59 13.726	+16 58 42.13	1	1	-0.29	0.25	K87
2024 8 15.854281	17 59 09.20	+16 58 39.4	1	1	-0.03	-0.71	Z80
2024 8 15.86281	17 59 07.817	+17 01 45.08	1	1	0.03	0.57	G34
2024 8 16.908094	17 56 12.427	+22 05 37.28	1	1	0.42	-0.32	Z80
2024 8 16.919223	17 55 53.02	+22 07 56.8	1	1	-0.18	0.58	G34
2024 8 16.919319	17 56 06.643	+22 08 29.15	1	1	-0.25	0.13	Z80
2024 8 16.924262	17 55 50.71	+22 09 10.9	1	1	0.21	-0.1	G34
2024 8 16.934328	17 55 46.26	+22 11 37.5	1	1	0.12	-0.82	G34
2024 8 17.847128	17 54 06.09	+26 04 54.0	1	1	-0.25	0.18	203
2024 8 17.866413	17 53 55.23	+26 09 12.6	1	1	-0.06	0.73	203
2024 8 19.829362	17 49 49.51	+32 53 05.6	1	1	0.06	0.28	G34
2024 8 19.836813	17 49 45.94	+32 54 22.5	1	1	-0.61	-0.55	G34

Continued on next page

Table A1 – *Continued from previous page*

Date ¹ (UTC)	R.A. ²	Dec. ³	$\sigma_{\text{R.A.}}$ ⁴ (")	$\sigma_{\text{Dec.}}$ ⁵ (")	$X_{\text{res.}}$ ⁶ (")	$Y_{\text{res.}}$ ⁷ (")	Obs. code ⁸
2024 8 19.844249	17 49 42.41	+32 55 37.3	1	1	0.04	-0.19	G34
2024 8 19.851685	17 49 38.86	+32 56 50.8	1	1	-0.1	-0.06	G34
2024 8 23.848972	17 42 22.905	+42 36 29.87	1	1	-0.07	0.02	Z84
2024 8 23.855223	17 42 19.625	+42 37 09.02	1	1	-0.03	-0.01	Z84
2024 8 27.82145	17 35 51.09	+48 46 30.6	1	1	-0.14	0.11	033
2024 8 27.8226	17 35 50.65	+48 46 35.0	1	1	0.1	-0.01	033
2024 8 27.82374	17 35 50.2	+48 46 39.5	1	1	-0.1	-0.07	033
2024 8 28.837555	17 34 24.755	+50 04 53.76	1	1	-0.24	-0.01	Z84
2024 8 28.847621	17 34 20.044	+50 05 29.17	1	1	-0.26	0.26	Z84
2024 8 28.858796	17 34 14.908	+50 06 06.48	1	1	0.12	0.53	Z84
2024 9 10.85884	17 20 37.5	+60 13 29.6	1	1	0.26	0.01	Y65
2024 9 10.86154	17 20 36.47	+60 13 32.6	1	1	0.16	0.12	Y66
2024 9 10.88186	17 20 28.45	+60 13 48.9	1	1	0.04	0.54	Y65
2024 9 10.89336	17 20 24.45	+60 13 56.6	1	1	0.82	0.52	Y65
2024 9 10.89497	17 20 23.77	+60 13 57.4	1	1	0.28	0.49	Y64
2024 9 10.90274	17 20 21.01	+60 14 01.3	1	1	0.09	-0.35	Y64
2024 9 10.90364	17 20 20.68	+60 14 02.1	1	1	-0.04	0.25	Y66
2024 9 10.90487	17 20 20.36	+60 14 02.6	1	1	-0.23	0.17	Y65
2024 9 10.91735	17 20 16.11	+60 14 06.8	1	1	0.59	0.55	Y65
2024 9 10.92688	17 20 13.07	+60 14 08.0	1	1	0.35	0.18	Y64
2024 9 10.92983	17 20 12.27	+60 14 07.9	1	1	0.55	0.16	Y65
2024 9 10.93531	17 20 10.52	+60 14 09.6	1	1	0.28	0.24	Y64
2024 9 10.94153	17 20 08.71	+60 14 09.8	1	1	-0.04	-0.08	Y66
2024 9 10.94332	17 20 08.32	+60 14 10.2	1	1	-0.33	0.45	Y64
2024 9 10.95033	17 20 06.39	+60 14 09.6	1	1	0.04	-0.51	Y64
2024 9 10.95741	17 20 04.60	+60 14 08.9	1	1	0.02	0.41	Y64
2024 9 10.96505	17 20 02.72	+60 14 07.8	1	1	-0.12	0.09	Y64
2024 9 10.97207	17 20 01.09	+60 14 06.0	1	1	-0.13	0.11	Y64
2024 9 10.97949	17 19 59.49	+60 14 04.6	1	1	0.53	-0.45	Y64
2024 9 11.84545	17 19 52.21	+60 45 30.9	1	1	0.33	-0.09	Y65
2024 9 11.85686	17 19 47.59	+60 45 43.7	1	1	0.25	0.15	Y65
2024 9 11.86086	17 19 45.98	+60 45 47.1	1	1	0.29	-0.08	Y66
2024 9 11.87988	17 19 38.65	+60 46 01.8	1	1	-0.39	0.28	Y65
2024 9 11.89139	17 19 34.52	+60 46 07.8	1	1	-0.01	0.18	Y65
2024 9 11.89536	17 19 33.04	+60 46 12.0	1	1	-0.13	-0.03	Y64
2024 9 11.93403	17 19 20.61	+60 46 17.6	1	1	0.34	0.01	Y65
2024 9 11.9409	17 19 18.68	+60 46 18.7	1	1	0.4	-0.39	Y66
2024 9 11.97274	17 19 10.92	+60 46 13.4	1	1	0.62	-0.79	Y64

Continued on next page

Table A1 – *Continued from previous page*

Date ¹ (UTC)	R.A. ²	Dec. ³	$\sigma_{\text{R.A.}}$ ⁴ (")	$\sigma_{\text{Dec.}}$ ⁵ (")	$X_{\text{res.}}$ ⁶ (")	$Y_{\text{res.}}$ ⁷ (")	Obs. code ⁸
2024 9 12.84336	17 19 01.18	+61 16 43.2	1	1	0.19	-0.17	Y65
2024 9 12.85477	17 18 56.48	+61 16 54.7	1	1	0.44	0.14	Y65
2024 9 12.86628	17 18 52.04	+61 17 03.7	1	1	0.2	-0.03	Y65
2024 9 12.87779	17 18 47.64	+61 17 11.8	1	1	0.5	-0.03	Y65
2024 9 12.8893	17 18 43.44	+61 17 17.4	1	1	0.06	-0.1	Y65
2024 9 12.90081	17 18 39.48	+61 17 21.3	1	1	0.09	-0.03	Y65
2024 9 12.91244	17 18 35.66	+61 17 23.7	1	1	-0.04	-0.22	Y65
2024 9 12.92782	17 18 30.86	+61 17 25.8	1	1	-0.78	-0.44	Y65
2024 9 13.8485	17 18 05.30	+61 47 03.9	1	1	-0.33	-0.68	Y65
2024 9 13.86754	17 17 57.79	+61 47 18.3	1	1	0.33	-0.67	Y65
2024 9 13.88793	17 17 50.3	+61 47 28.7	1	1	-0.05	0.33	Y65
2024 9 15.84434	17 16 10.55	+62 44 45.7	1	1	-0.21	0.05	Y65
2024 9 15.86338	17 16 03.04	+62 44 58.2	1	1	0.09	-0.04	Y65
2024 9 15.88376	17 15 55.46	+62 45 06.3	1	1	0.01	0.04	Y65
2024 9 17.84365	17 13 58.4	+63 38 52.7	1	1	-0.16	-0.74	Y65
2024 9 17.86082	17 13 51.66	+63 39 01.1	1	1	-0.22	0.35	Y65
2024 9 20.86196	17 09 58.04	+64 52 53.6	1	1	0.21	-0.18	Y65
2024 9 20.87734	17 09 52.26	+64 52 55.3	1	1	-0.01	-0.04	Y65
2024 9 20.89048	17 09 47.64	+64 52 53.7	1	1	0.16	-0.02	Y65
2024 9 21.84305	17 08 39.12	+65 15 27.1	1	1	0.41	0.01	Y65
2024 9 21.86478	17 08 30.58	+65 15 30	1	1	0.52	0.36	Y65
2024 9 21.88966	17 08 21.65	+65 15 26.4	1	1	0.44	0.27	Y65
2024 9 22.84114	17 07 10.0	+65 37 03.7	1	1	0.05	0.14	Y65
2024 9 22.86519	17 07 00.66	+65 37 04.4	1	1	0.23	0.05	Y65
2024 9 23.84203	17 05 36.94	+65 57 41.1	1	1	0.14	-0.37	Y65
2024 9 23.87183	17 05 25.56	+65 57 39.0	1	1	0.22	-0.21	Y65
2024 9 24.83839	17 04 03.45	+66 17 22.4	1	1	0.06	0.06	Y65
2024 9 24.85555	17 03 56.71	+66 17 21.9	1	1	0.2	0.14	Y65
2024 9 24.87203	17 03 50.62	+66 17 18.2	1	1	-0.15	0.19	Y65
2024 9 25.8363	17 02 27.43	+66 36 11.3	1	1	0.3	-0.58	Y65
2024 9 25.85233	17 02 21.15	+66 36 09.6	1	1	-0.18	-0.03	Y65
2024 9 25.86847	17 02 15.17	+66 36 05.0	1	1	-0.28	-0.35	Y65
2024 9 26.83482	17 00 49.93	+66 54 10.9	1	1	-0.31	-0.34	Y65
2024 9 26.85011	17 00 43.91	+66 54 08.8	1	1	-0.39	-0.31	Y65
2024 9 26.8655	17 00 38.26	+66 54 04.2	1	1	-0.02	0.35	Y65
2024 9 26.88634	17 00 31.16	+66 53 54.6	1	1	0.38	0.4	Y65
2024 9 26.90718	17 00 25.01	+66 53 40.9	1	1	0.52	0.44	Y65
2024 9 26.95133	17 00 14.74	+66 53 06.0	1	1	0.03	0.01	Y65

Continued on next page

Table A1 – *Continued from previous page*

Date ¹ (UTC)	R.A. ²	Dec. ³	$\sigma_{\text{R.A.}}$ ⁴ (")	$\sigma_{\text{Dec.}}$ ⁵ (")	$X_{\text{res.}}$ ⁶ (")	$Y_{\text{res.}}$ ⁷ (")	Obs. code ⁸
2024 9 27.24615	16 59 59.22	+67 01 25.5	1	1	-0.07	0.27	T15
2024 9 27.25283	16 59 56.71	+67 01 22.3	1	1	-0.01	0.31	T15
2024 9 27.25901	16 59 54.45	+67 01 19.0	1	1	-0.05	0.35	T15
2024 9 27.83397	16 59 11.15	+67 11 26.6	1	1	-0.14	0.52	Y65
2024 9 27.83856	16 59 09.4	+67 11 25.9	1	1	0.05	0.32	Y66
2024 9 27.84556	16 59 06.71	+67 11 24.4	1	1	-0.25	0.13	Y64
2024 9 27.853	16 59 03.82	+67 11 21.8	1	1	0.17	0.14	Y65
2024 9 27.86662	16 58 58.9	+67 11 16.8	1	1	0.06	-0.11	Y66
2024 9 27.8687	16 58 58.19	+67 11 15.9	1	1	-0.41	0.21	Y64
2024 9 27.87868	16 58 54.83	+67 11 10.9	1	1	-0.26	0.15	Y65
2024 9 27.89084	16 58 50.98	+67 11 03.9	1	1	-0.36	0.25	Y64
2024 9 27.89679	16 58 49.24	+67 10 59.8	1	1	-0.27	0.29	Y66
2024 9 27.91348	16 58 44.6	+67 10 47.5	1	1	0.29	0.26	Y64
2024 9 28.83442	16 57 31.24	+67 28 00.7	1	1	-0.08	0.52	Y65
2024 9 28.88381	16 57 13.72	+67 27 39.0	1	1	-0.11	0.19	Y65
2024 9 28.89529	16 57 11.15	+67 27 36.2	1	1	0.01	0.15	950
2024 9 28.90177	16 57 09.31	+67 27 31.6	1	1	0.04	0.19	950
2024 9 28.90825	16 57 07.51	+67 27 26.9	1	1	0.21	-0.13	950
2024 9 28.91473	16 57 05.83	+67 27 21.9	1	1	0.02	0.06	950
2024 9 28.92122	16 57 04.32	+67 27 16.6	1	1	0.27	-0.54	950
2024 9 28.9277	16 57 02.74	+67 27 11.4	1	1	0.24	-0.19	950
2024 9 29.82906	16 55 53.02	+67 44 00.0	1	1	0.15	-0.32	Y65
2024 9 29.84847	16 55 45.62	+67 43 53.9	1	1	0.23	0.01	Y65
2024 10 1.83749	16 52 27.89	+68 14 20.4	1	1	0.27	-0.04	Y65
2024 10 1.85973	16 52 20.02	+68 14 08.9	1	1	0.66	-0.17	Y65
2024 10 1.88199	16 52 12.98	+68 13 54.1	1	1	0.24	-0.16	Y65
2024 10 4.83929	16 47 19.41	+68 56 55.2	1	1	-0.75	0.48	Y65
2024 10 4.88548	16 47 05.0	+68 56 22.5	1	1	0.21	0.18	Y65
2024 10 4.93239	16 46 54.96	+68 55 37.7	1	1	0.27	-0.04	Y65
2024 10 5.84908	16 45 31.01	+69 10 26.6	1	1	0.66	-0.17	Y65
2024 10 5.88813	16 45 19.54	+69 09 55.9	1	1	0.24	-0.16	Y65
2024 10 5.92928	16 45 11.08	+69 09 15.9	1	1	-0.75	0.48	Y65
2024 10 7.88296	16 41 45.06	+69 36 32.0	1	1	0.21	0.18	Y65
2024 10 7.89237	16 41 42.59	+69 36 23.9	1	1	0.62	-0.09	Y65
2024 10 8.82832	16 40 09.68	+69 50 13.4	1	1	-0.11	-0.55	Y65
2024 10 8.84586	16 40 03.75	+69 50 01.4	1	1	0.44	0.34	Y65
2024 10 8.86173	16 39 58.69	+69 49 48.6	1	1	0.62	-0.09	Y65
2024 10 9.84523	16 38 08.18	+70 02 50.4	1	1	-0.11	-0.55	Y65

Continued on next page

Table A1 – *Continued from previous page*

Date ¹ (UTC)	R.A. ²	Dec. ³	$\sigma_{\text{R.A.}}$ ⁴ (")	$\sigma_{\text{Dec.}}$ ⁵ (")	$X_{\text{res.}}$ ⁶ (")	$Y_{\text{res.}}$ ⁷ (")	Obs. code ⁸
2024 10 9.88126	16 37 57.91	+70 02 18.8	1	1	0.44	0.34	Y65
2024 10 9.91815	16 37 50.18	+70 01 42.8	1	1	0.6	-0.53	Y65
2024 10 10.88056	16 35 58.18	+70 14 55.4	1	1	-0.34	0.19	Y65
2024 10 10.91746	16 35 50.83	+70 14 18.0	1	1	-0.31	-0.31	Y65
2024 10 14.84781	16 27 15.74	+71 03 22.0	1	1	0.1	-0.55	Y65
2024 10 14.89339	16 27 04.32	+71 02 35.6	1	1	-0.75	-0.02	Y65
2024 10 18.84606	16 16 51.1	+71 44 58.1	1	1	-0.38	-0.23	Y65
2024 10 18.88508	16 16 41.38	+71 44 12.4	1	1	0.22	0.72	Y65
2024 10 19.8438	16 14 03.17	+71 54 01.4	1	1	-0.54	-0.11	Y66
2024 10 22.85193	16 05 19.37	+72 17 31.3	1	1	-0.02	0.21	Y65
2024 10 22.87034	16 05 15.17	+72 17 09.0	1	1	-0.3	-0.46	Y65
2024 10 24.84329	15 59 28.11	+72 31 02.0	1	1	0.62	-0.24	Y65
2024 10 24.85969	15 59 24.31	+72 30 40.0	1	1	-0.1	-0.22	Y65

Table A1. Columns: (1) UTC observation date at the mid-point of the exposure; (2) right ascension; (3) declination; (4) uncertainty in right ascension; (5) uncertainty in declination; (6) observed-minus-computed residual in the X direction; (7) observed-minus-computed residual in the Y direction; (8) Minor Planet Center Observatory Code